Available online at www.sciencedirect.com
SCIENCE DIRECT
Journal of Molecular Catalysis A: Chemical 245 (2006) 106–113
JOURNAL OF MOLECULAR CATALYSIS A: CHEMICAL
www.elsevier.com/locate/molcata

Characterization and catalytic performances of supported chromia catalysts for C_{10}+ heavy aromatics hydrodealkylation

Dexian Shi, Zhen Zhao *, Chunming Xu, Aijun Duan, Jian Liu, Tao Dou

State Key Laboratory of Heavy Oil Processing, China University of Petroleum, Beijing 102249, China

Received 26 June 2005; received in revised form 23 September 2005; accepted 23 September 2005
Available online 27 October 2005

Abstract

Al_2O_3 and SiO_2 were used to load chromium oxides with incipient-wetness impregnation method. These supported chromia catalysts were evaluated for the dealkylation of C_{10}+ heavy aromatics in hydrogen flow and were characterized with BET, XRD, UV–vis DRS and H_2-TPR techniques. The results indicate that the catalytic activity of supported chromia catalysts on SiO_2 is higher than that of on Al_2O_3. Structural characterization results show that surface reduced CrO_x species are the active sites for hydrodealkylation of C_{10}+ heavy aromatics. (C_{10}+ heavy aromatics denote the aromatics whose carbon numbers are equal to or greater than 10.) The structural models of CrO_x species on the Al_2O_3 or SiO_2 support surface were also proposed.

Keywords: C_{10}+ heavy aromatics; Catalysts; CrO_x; Hydrodealkylation; Characterization; Structural model

1. Introduction

Aromatics are widely used as key and basic feedstocks of petrochemical industry. The demand for aromatics (mainly BTX, i.e. benzene, toluene and xylene) remains strong, and in this case, reforming and aromatization were widely used to meet the demand. Accompanying with the light aromatics, heavy aromatics with carbon numbers equal to or more than 10 are generated. They are rarely used and often burned off as fuels, which is a great waste of aromatic resources. Hydrodealkylation has attracted much more attention as a candidate method for heavy aromatics utilization. This method to get light aromatics is through the scission of subchain of alkyl aromatics in H_2 atmosphere thermally or catalytically. Catalytic process takes place at lower temperature compared to the thermal one. Several catalytic processes have been developed since the method was put into practice and little change has been taken place on the arts and crafts. The major problem lies in the development of new types of catalysts.

Some catalysts have been developed [1–15] for treating feedstocks containing C_9 (or C_7,C_8) aromatics .The dealkylation performances on different catalysts were also studied [16–18] and most of them used model compounds. But the actual feeds are mixed aromatics compounds and they may have different performances in hydrodealkylation process. As far as we know, few papers in open literature converted hydrodealkylation catalysts for C_{10}+ aromatics, and there is also no report on the correlating the molecular structure of supported chromia catalysts and their catalytic performances for the hydrodealkylation of heavy aromatics.

In this study, several systems of supported chromia catalysts were prepared by incipient-wetness impregnation method. BET, XRD, UV–vis DRS and H_2-TPR techniques were used to characterize their structures and physico-chemical properties. The fundamental insight into the molecular structure of the supported chromia catalysts and their reactivity/selectivity relationship was obtained.

2. Experimental

2.1. Catalyst preparation

The Catalyst samples were prepared by an incipient-wetness impregnation method with aqueous solutions of $Cr(NO_3)_3{\cdot}9H_2O$. The oxide supports were Al_2O_3 (provided by Shandong Aluminium Co. LTD, Analytical grade, pore volume

* Corresponding author. Tel.: +86 10 89731586; fax: +86 10 89731586.
E-mail address: zhenzhao@cup.edu.cn (Z. Zhao).

1381-1169/$ – see front matter © 2005 Elsevier B.V. All rights reserved.
doi:10.1016/j.molcata.2005.09.031

0.26 ml/g and BET specific surface area is 179 m^2/g), SiO_2 (provided by Qingdao Haiyang Chemical Co., Ltd & Spegial Silica Gel Factory, Macro-pored Micro-spherical Silica Gel, pore volume 0.94 ml/g and BET specific surface area is 342 m^2/g). After the impregnation step, the samples were dried at room temperature for 2 h and at 120 °C overnight. Finally, the catalysts were calcined in air at 600 °C for 4 h. The Cr content is expressed as the density of Cr atom on surface of support i.e., Cr/nm^2.

2.2. Catalyst characterization methods

The BET specific surface areas of the studied samples were measured with linear parts of the BET plot of the N_2 isotherms, using a Micromeritics ASAP 2010 analyzer.

Powder X-ray diffraction was performed on Shimadzu XRD 6000 diffraction-meter, operating at 40 KV and 10 mA, using Cu Kα (λ = 1.54184 Å) radiation combined with nickle filter. The diffraction data were recorded for 2θ values between 20° and 50° and the scanning rate was 8° min^{-1}.

Diffuse reflectance ultraviolet–visible diffuse reflectance spectra (UV–vis DRS) of the catalysts were performed on a HITACHI U-4100 UV–vis NIR spectrophotometer. The spectra were collected from 200 to 800 nm and referenced with carrier under ambient conditions.

The TPR measurement was carried out in a micro-reactor containing ca. 0.2 g of catalyst that was attached to GC analyzer. The catalysts were pretreated at 600 °C for 1 h in an air flow. Helium was used as the carrier gas. A 10% H_2/He (v/v) mixture flowing at 40 ml/min was used for reduction and the temperature was ramped at a rate of 10 °C/min from 50 to 700 °C. Hydrogen consumption was determined with a TCD.

After H_2-TPR, the reduced samples were mixed with carrier, and then the mixture were put into the DR-cell of the UV–vis spectrometer to get the DRS spectra.

2.3. Activity test

The catalytic activity was tested in a continuous experimental system, which included a stainless steel reactor with 8 mm inner diameter, an electrical furnace, a cooler, a gas–liquid separator, and a high pressure liquid pump. The catalysts with size ranging from 40 to 80 mesh were put in the reactor. The reactor temperature was under automatic control. The hydrogen gas was supplied by a high pressure commercial cylinder. The catalytic performances of all the prepared catalysts for hydrodealkylation of C_{10}+ heavy aromatics which were directly gotten from industry unit were investigated. The H_2 used in the experiments was gotten from Jinggao gas corporation, and its purity is 99.99 wt.%.

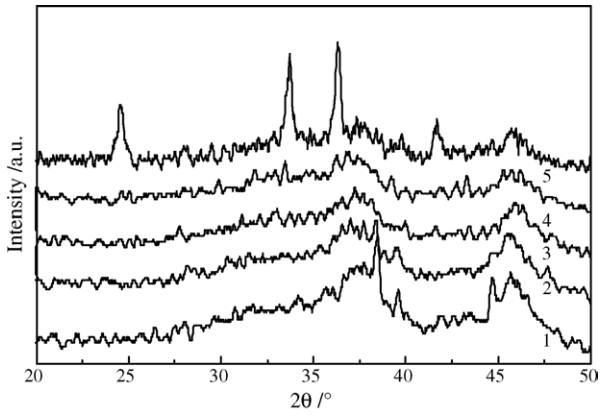

Fig. 1. XRD patterns of Cr_2O_3/Al_2O_3 samples. Cr contents is (1) 1.65 Cr/nm^2, (2) 4.41 Cr/nm^2, (3) 7.17 Cr/nm^2, (4) 11.03 Cr/nm^2, and (5) 14.89 Cr/nm^2.

3. Results and discussion

3.1. BET surface area analysis

The surface areas of the Al_2O_3- and SiO_2-supported chromium oxide catalysts are listed in Table 1. The specific surface area of CrO_x/SiO_2 catalyst slightly decreases with the increasing chromium loading as Cr contents is less than 1.17 Cr/nm^2, but the surface area decreases rapidly when it is greater than 1.17 Cr/nm^2. For CrO_x/Al_2O_3 system, the surface area increases to 195 m^2/g when Cr/Al molar ratio is equal to 0.55 Cr/nm^2, it keeps almost constant for Cr contents from 4.41 to 7.17 Cr/nm^2.

3.2. XRD results

The XRD patterns of CrO_x/Al_2O_3 and CrO_x/SiO_2 are exhibited in Figs. 1 and 2, respectively.

From Fig. 1, when Cr contents are lower than 11.03 Cr/nm^2, no Cr_2O_3 characteristic diffraction peak was detected. As Cr content equals to 11.03 Cr/nm^2 very weak diffraction peaks of crystalline Cr_2O_3 are observed. These results suggest that the

Table 1
BET surface area of CrO_x supported catalysts

SiO_2			Al_2O_3		
Cr/Si (mol%)	Cr contents (Cr/nm^2)	BET SA (m^2/g)	Cr/Al (mol%)	Cr contents (Cr/nm^2)	BET SA (m^2/g)
0	0	342	0	0	179
0.5	0.15	341	1	0.55	195
1	0.29	337	3	1.65	167
2	0.59	335	8	4.41	118
4	1.17	327	11	6.06	119.6
12	3.52	276	13	7.17	119
20	5.87	257	27	14.89	102

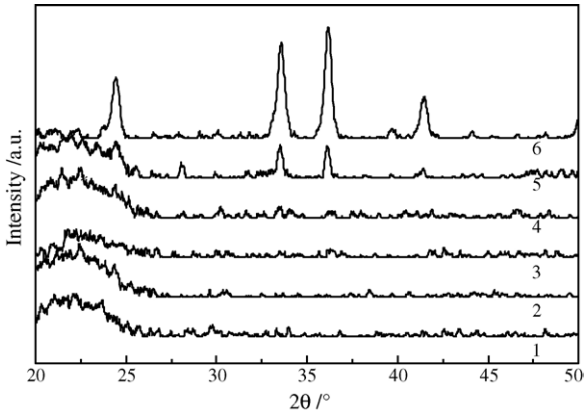

Fig. 2. XRD pattern of CrO_x/SiO_2 samples. Cr contents is (1) 0 Cr/nm^2, (2) 0.15 Cr/nm^2, (3) 0.29 Cr/nm^2, (4) 0.59 Cr/nm^2, (5) 1.17 Cr/nm^2, and (6) 5.87 Cr/nm^2.

CrO_x species on Al_2O_3 are well dispersed and exist in an amorphous state when the loading amount is less than 11.03 Cr/nm^2.

From Fig. 2, when Cr content equals to 0.59 Cr/nm^2, very weak Cr_2O_3 characteristic diffraction peaks can be detected. If the Cr concentrations is below 0.59 Cr/nm^2, the XRD patterns are very similar to that of SiO_2, indicating that the CrO_x species exist in a dispersive or amorphous states.

3.3. TPR results

3.3.1. CrO_x/Al_2O_3

Fig. 3 shows the TPR curves of CrO_x/Al_2O_3 catalysts and the corresponding TPR results of the samples are listed in Table 2. It can be seen that H_2 consumption peak at about 377 °C was detected for the sample with Cr content of 0.55 Cr/nm^2, which is ascribed to the reduction of Cr^{6+} to Cr^{3+}. The T_{onset} and T_{max} of this reduction peak downshifts to the lower temperature with the increasing of Cr content. At the Cr contents of 2.76, 4.41 and 6.06 Cr/nm^2, there also appear reduction peaks at around 529 °C, which may generate from the reduction of Cr^{6+} that has strong interaction with the carrier [19,20]. These two peaks may

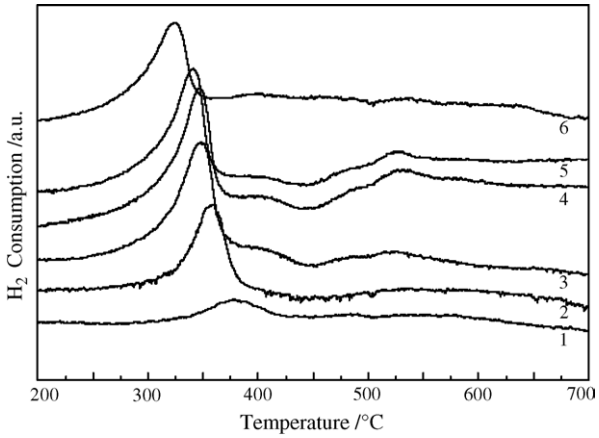

Fig. 3. H_2-TPR spectra of CrO_x/Al_2O_3 samples. Cr contents is (1) 0.55 Cr/nm^2, (2) 1.65 Cr/nm^2, (3) 2.76 Cr/nm^2, (4) 4.41 Cr/nm^2, (5) 6.06 Cr/nm^2, and (6) 14.89 Cr/nm^2.

Table 2
TPR results of CrO_x/Al_2O_3 samples

Cr contents (Cr/nm^2)	T_{onset} (°C)	$T_{max(1)}$ (°C)	$T_{max(2)}$ (°C)	Total area of TPR peaks (a.u.)
0.55	339	377		366
1.65	320	359		527
2.76	244	348	526	725
4.41	230	347	532	924
6.06	224	341	529	803
11.03	207	323		931

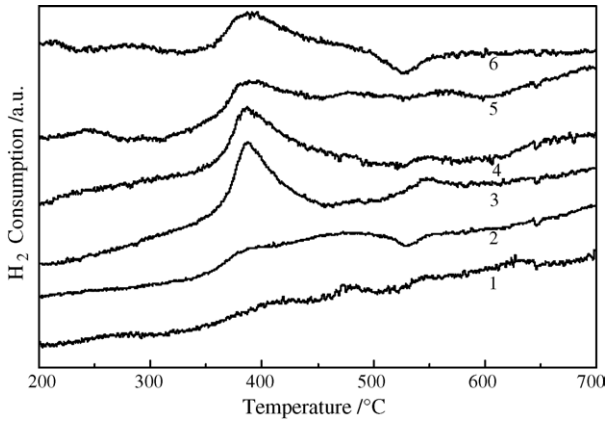

Fig. 4. H_2-TPR spectra of CrO_x/SiO_2 samples. Cr contents is (1) 0.15 Cr/nm^2, (2) 0.29 Cr/nm^2, (3) 0.59 Cr/nm^2, (4) 1.17 Cr/nm^2, (5) 2.35 Cr/nm^2, and (6) 3.52 Cr/nm^2.

relate to the reduction of the two types of surface CrO_x species near to the monolayer coverage. No reduction peak was detected as temperature was higher than 550 °C.

3.3.2. CrO_x/SiO_2

Fig. 4 shows the TPR curves of CrO_x/SiO_2 catalysts and the corresponding results are listed in Table 3. In the curve of Cr content of 0.15 Cr/nm^2, a weak H_2 consumption peak presents at about 390 °C, and its T_{onset} is at about 371 °C. With the Cr content increasing to 0.29 mol%, the T_{onset} and T_{max} are at a constant value of 356 and 387 °C, respectively, and the peak at around 400 °C become wider. This may be due to the similar interaction between chromia and the carrier. The value of the H_2 consumption area of the peaks corresponds to the Cr^{6+} amounts on the carrier. This may be the result from monolayer coverage. The weak consumption peak at about 550 °C may be assigned

Table 3
TPR results of CrO_x/SiO_2 samples

Cr contents (Cr/nm^2)	T_{onset} (°C)	$T_{max(1)}$ (°C)	$T_{max(2)}$ (°C)	Total area of TPR peaks (a.u.)
0.15	371	390		110
0.29	356	387		370
0.59	356	387	548	509
1.17	356	387	548	567
2.35	357	389		748
3.52	356	387		368

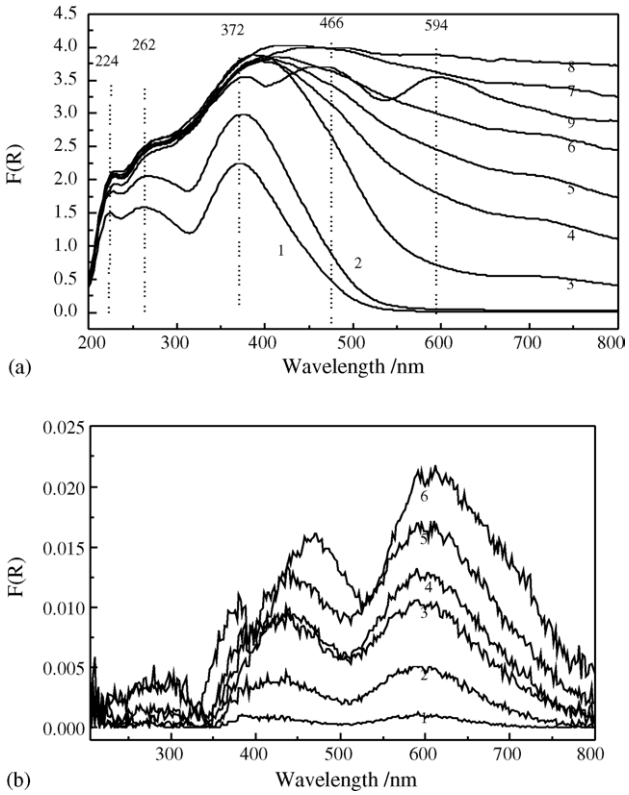

Fig. 5. UV–vis DRS spectra of CrO_x/Al_2O_3 samples: (a) before TPR reduction, (b) after TPR reduction. Cr contents in Fig. 7a is (1) 0.16 Cr/nm^2, (2) 0.55 Cr/nm^2, (3) 1.65 Cr/nm^2, (4) 2.76 Cr/nm^2, (5) 4.41 Cr/nm^2, (6) 6.06 Cr/nm^2, (7) 7.17 Cr/nm^2, (8) 11.03 Cr/nm^2, and (9) 14.89 Cr/nm^2. Cr contents in Fig. 7b is (1) 0.55 Cr/nm^2, (2) 1.65 Cr/nm^2, (3) 2.76 Cr/nm^2, (4) 4.41 Cr/nm^2, (5) 6.06 Cr/nm^2, and (6) 14.89 Cr/nm^2.

to the reduction of Cr^{6+} ions, which has a stronger interaction with the support [19,20].

From CrO_x/Al_2O_3 and CrO_x/SiO_2 systems, it can be found that at around monolayer coverage, the H_2 consumptions have some special features, which may have the largest amount of the surface CrO_x species.

According to the TPR plots in Figs. 3 and 4, CrO_x loaded on the two carriers all have two H_2 consumption peaks. The first peak with reduction temperature less than 400 °C may come from the reduction of CrO_x species that have a weak interaction with the carrier. However, the second one is due to that of CrO_x species that have strong interactions with the carrier.

In general, H_2-TPR results indicate that under the reaction conditions the CrO_x species on the two carriers have been reduced, mainly existing as the three valence Cr [21], which was also confirmed by our UV–vis measurement results in the following sections.

3.4. UV–vis DRS results

3.4.1. CrO_x/Al_2O_3

The UV–vis DRS spectra of CrO_x/Al_2O_3 catalysts before and after TPR are presented in Fig. 5a and b, respectively.

In Fig. 5a, the bands around 262 and 372 nm for Cr content 0.16 Cr/nm^2, are assigned to the charge transfers of $O^{2-} \rightarrow Cr^{6+}$ [23]. With Cr-loading increasing the absorbance edge red shifted when Cr-loading below 6.06 Cr/nm^2. The band around 224 nm may result from the interaction between Cr and the support in all the spectra [24]. As the Cr content is over 1.65 Cr/nm^2, the absorbance intensity has little difference among all the samples, which indicates that the amount of surface Cr^{6+} species are almost the same. The absorbance band around 466 nm is attributed to dichromate. And the bands from 550 to 800 nm and centered at around 594 nm is the absorbance of d–d electron transition of (pseudo)octahedral Cr^{3+} or Cr_2O_3 .For the samples with chromium loading below 0.55 Cr/nm^2, no Cr^{3+} was detected, while the intensity of the absorbance band from 550–800 nm greatly increases with chromium loading increasing, suggesting the enhancement of Cr^{3+} content with chromium loading.

In Fig. 5b, the absorbance bands that exist in Fig. 5a can also be observed, but their relative intensities are different from those before reduction. The intensity ratio of the bands centering at 600 nm to the bands below 350 nm greatly increases. This is due to the reduction of higher valence CrO_x species. For the absorbance bands below 350 nm, the absorbance intensity of the catalyst containing 0.16 Cr/nm^2 is the highest among the prepared catalysts. This is because that the lower Cr loading catalysts have more monochromate which are more difficult to be reduced compared to the higher Cr loading catalysts in which polychromium oxide are mainly present. Therefore, the catalysts with isolated chromium oxide structure are more difficult to be reduced than those with polymeric chromium oxide structure.

UV–vis diffuse reflectance spectroscopy has been widely used to investigate the structures and the oxidation states of metal-containing solid oxides that possess the ligand-to-metal charge transfer (LMCT) transition of high valence in the region of 400–200 nm and d–d transitions of low valence ions in the range of 600–800 nm. For the chromium catalyst the bands of 200–333 and 530–800 nm are the characteristic absorption bands for Cr^{6+} and Cr^{3+}, respectively. Therefore, the ratio of the d–d electron transition band area of Cr^{3+}(530–800 nm) to the area of LMCT band of Cr^{6+} (200–330 nm) was chosen as a parameter to relatively quantify the reduction extent of Cr^{6+} cations in this study [22].

The ratio of d–d transition band area of Cr^{3+} (530–800 nm) to the band area of charge transfer of Cr^{6+} (200–333 nm) of CrO_x/Al_2O_3 before and after TPR was calculated [22] and listed in Table 4.

Table 4
The ratio of d–d transition band area of Cr^{3+} (530–800 nm) to the band area of charge transfer of Cr^{6+} (200–333 nm) of CrO_x/Al_2O_3 before and after TPR

Cr contents (Cr/nm^2)	Ratio before TPR	Ratio after TPR
0.55	0.05	0.29
1.65	0.55	2.01
2.76	1.39	9.58
4.41	1.97	19.67
6.06	2.45	41.76
14.89	2.93	40.05

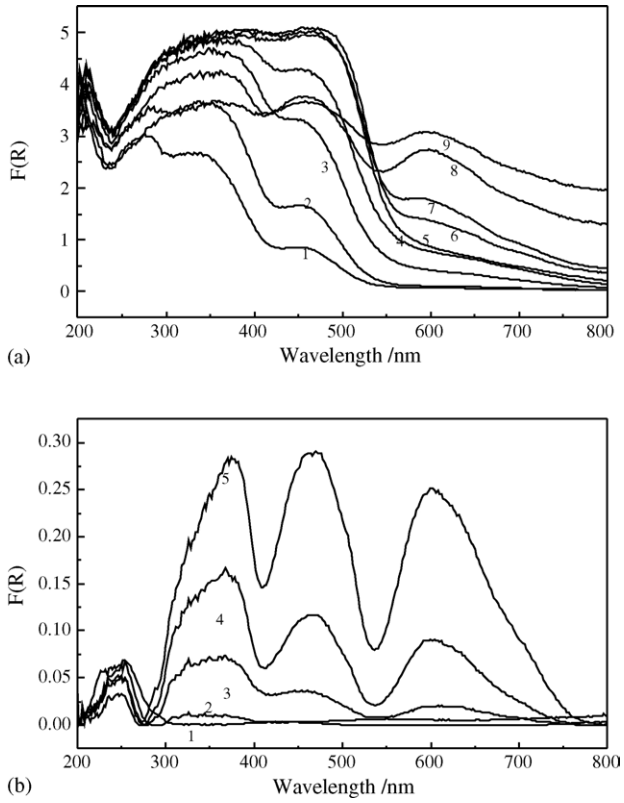

Fig. 6. UV–vis DRS spectra of CrO_x/SiO_2 samples: (a) before TPR, (b) after TPR. Cr contents in Fig. 8a is (1) 0.015 Cr/nm^2, (2) 0.03 Cr/nm^2, (3) 0.07 Cr/nm^2, (4) 0.15 Cr/nm^2, (5) 0.29 Cr/nm^2, (6) 0.59 Cr/nm^2, (7) 1.17 Cr/nm^2, (8) 3.52 Cr/nm^2, and (9) 5.87 Cr/nm^2. Cr contents in Fig. 8b is (1) 0.15 Cr/nm^2, (2) 0.29 Cr/nm^2, (3) 0.59 Cr/nm^2, (4) 1.17 Cr/nm^2, and (5) 3.52 Cr/nm^2.

From Table 4, it can be found that some amounts of Cr^{3+} are present on the CrO_x/Al_2O_3 samples even if before TPR. Moreover, Cr^{3+} content increases with chromium loading increasing. For the same sample, the ratio value after TPR are much greater than that before TPR indicating that a large amounts of Cr^{6+} were reduced to Cr^{3+} during TPR process. With the Cr content increasing the ratio value rapidly increase, which demonstrates that the isolated chromate is more difficult to be reduced than polymerized chromate oxide species.

3.4.2. CrO_x/SiO_2

Fig. 6a and b shows the UV–vis DRS spectra of CrO_x/SiO_2 catalysts before and after TPR. For Cr loading less than 0.03 Cr/nm^2, two intense bands are observed at ca. 270 and 370 nm. These bands are generally assigned to $O^{2-} \rightarrow Cr^{6+}$ charge transfer transition of monochromate species. The figure also shows a band at ca. 460 nm, which is usually ascribed to Cr^{6+} in the chromate or the dichromate arrangement in contact with the support. For the sample with Cr content of 0.07 Cr/nm^2, a weak band at around 600 nm is present, which is usually assigned to a d–d transition of Cr^{3+} ions in a strongly distorted octahedral crystal field. These Cr^{3+} ions are present in a cluster of chromium oxide which was not detected by XRD since the sample was amorphous. As the Cr content increases to 0.29 Cr/nm^2, the intensity of the three bands below 550 nm continue to increase.

Table 5
The ratio of the band area of d–d transition of Cr^{3+} (530–800 nm) to the band area of charge transfer band area of Cr^{6+} (200–278 nm) of CrO_x/SiO_2 before and after TPR

Cr contents (Cr/nm^2)	Ratio before TPR	Ratio after TPR
0.15	0.58	0.51
0.29	0.71	0.05
0.59	1.18	1.30
1.17	1.00	5.11
3.52	2.15	28.20

When the Cr content reaches 0.59 Cr/nm^2, the band intensities at ca. 270, 370, 460 nm decrease. The band intensity at about 600 nm continues to increase as the Cr loading increase from 0.015 to 5.87 Cr/nm^2 indicating the increasing of Cr^{3+} content.

The UV–vis DRS spectra of the CrO_x/SiO_2 catalysts after H_2-TPR are presented in Fig. 6b. It can be seen that a band centered at ca. 250 nm appeared and its intensity increases as the Cr loading decreases. This is because that the isolated CrO_x is difficult to be reduced. The band area ratios of the band centered at around 600 nm to the band from 200 to 278 nm are much greater than those of samples before TPR with Cr loading more than 0.59 Cr/nm^2, as shown in Table 5, demonstrating the reduction of $Cr^{6+} \rightarrow Cr^{3+}$. This ratio decreases after TPR which may be due to the reduction changes the environment of the supported chromia and causes the absorbance intensity decreasing in the bands 530–800 nm.

3.5. Catalytic activity

The catalytic activity and selectivity results of Al_2O_3 and SiO_2-supported chromia catalysts for hydrodealkylation of C_{10}+ heavy aromatics are listed in Tables 6 and 7, respectively.

From Table 6, the conversion of C_{10}+ aromatics increases with the increasing of Cr loading when Cr loading is less than 2.76 Cr/nm^2. For Cr loading from 2.76 to 6.06 Cr/nm^2 the conversion keeps almost constant. But the C_{10}+ conversion decreases gradually with the further increasing Cr loading. It is more likely that the surface CrO_x species on the carrier are the active species. And Cr_2O_3 crystalline surface may have lower dealkylation activity, which may cause the increase of selectivity. When Cr loading is greater than 11.03 Cr/nm^2, the characteristic diffraction peaks of crystalline Cr_2O_3 can be observed in the XRD patterns, and Cr_2O_3 characteristic vibration absorbance band can also be found in the FT-IR spectra (not be shown here). Moreover, the absorbance intensity of ca. 600 nm reach its maximum in UV–vis DRS spectra. The minimum size of crystal detected by XRD is about 4 nm [25]. Al_2O_3 has intense IR vibration absorbances in the range of which the IR vibration absorbance position of Cr_2O_3 locates. Therefore, the vibration band of CrO_x species on Al_2O_3 surface may be covered by those of Al_2O_3. Thus, it cannot confirm that at around 11.03 Cr/nm^2 loading is the monolayer coverage. According to Maymol et al. [26], 8 mol% Cr is the monolayer coverage, at which the highest activity for hydrodealkylation of C_{10}+ heavy aromatics in our study in the Al_2O_3 series was obtained. So it may guess that

Table 6
Catalytic performances of CrO_x/Al_2O_3 catalysts for C_{10}+ aromatics hydrodealkylation

Cr contents (Cr/nm^2)	Product distribution						C_8^- selectivity (mol%)	C_9^- selectivity (mol%)	C_{10}+ conversion (mol%)	Unit surface area conversion (mol%)
	C_6 (mol%)	C_7 (mol%)	C_8 (mol%)	C_9 (mol%)	C_8^- (mol%)	C_9^- (mol%)				
0	0.11	0.9	3.6	11.05	4.61	15.66	25.7	78	21.9	0.122
0.55	0.18	1.54	6.36	16.8	8.08	24.88	20.3	85	30.9	0.158
1.65	0.34	2.71	10.15	21.53	13.2	34.73	33.7	80.7	41.3	0.247
2.76	0.44	3.42	12.04	22.78	15.89	38.67	35.9	79.4	48.8	
4.41	0.55	3.78	12.19	22.24	16.53	38.77	36.2	77.3	49.7	0.421
6.06	0.43	3.00	10.8	22.82	14.24	37.05	31.6	74.5	48.6	0.406
7.15	0.42	3.22	11.05	20.22	14.69	34.91	32.9	73.3	46.3	0.389
11.03	0.4	2.71	9.85	22.34	12.97	35.31	37.6	88.9	42.3	
14.89	0.33	2.19	8.17	20.26	10.69	30.95	35.3	90.4	39	0.382

Table 7
Catalytic performances of CrO_x/SiO_2 catalysts for C_{10}+ aromatics hydrodealkylation

Cr contents (Cr/nm^2)	Product distribution						C_8^- selectivity (mol%)	C_9^- selectivity (mol%)	C_{10}+ conversion (mol%)	Unit surface area conversion (mol%)
	C_6 (mol%)	C_7 (mol%)	C_8 (mol%)	C_9 (mol%)	C_8^- (mol%)	C_9^- (mol%)				
0	0.13	1.14	4.56	15.02	5.83	20.85	25.0	98.6	23.3	0.068
0.15	0.15	1.26	4.53	15.68	5.94	21.62	31.2	91.4	34.0	0.1
0.29	0.48	3.28	10.86	25.32	14.62	39.94	36.6	87.5	47.8	0.142
0.59	0.49	3.52	12.55	27.53	16.56	44.09	38.2	91.9	50.7	0.151
1.17	0.62	4.40	10.36	24.83	16.17	42.61	38.7	90.9	49.3	0.151
2.35	0.50	3.66	12.57	26.81	16.73	43.54	38.6	90.8	50.5	
3.52	0.64	4.52	10.91	26.95	16.73	43.54	36.2	87.9	51.2	0.186
4.71	1.09	4.21	12.39	25.70	17.70	43.39	38.7	89.5	51.3	
5.87	0.55	3.72	12.26	26.67	16.52	43.19	33. 3	89.3	50.3	0.196

on Al_2O_3 surface when Cr loading exceed 4.41 Cr/nm^2 but less than 11.03 Cr/nm^2, Cr_2O_3 may exist in amorphous, two or more layers, but not in crystal form.

From Table 7, for the catalysts whose Cr loadings are less than 0.59 Cr/nm^2, the C_{10}+ conversion increases with the Cr-loading increasing, while the selectivity of C_9-slightly decreases. If the Cr-loading exceeds 0.59 Cr/nm^2, the C_{10}+ conversion and the selectivity of C_9 become almost constant as the Cr content increasing. From the above characterization results it can draw a conclusion that the monolayer coverage is around 0.59 Cr/nm^2 over the SiO_2 support, which is in good agreement with the literature [26]. And it can be easily characterized with UV–vis DRS and XRD. It can also be concluded that surface reduced CrO_x species on carrier surface are the active species since the C_{10}+ conversion increases with the increasing content of surface reduced CrO_x species. Because SiO_2 has high surface area, the increasing Cr loading may not cause much difference in the characteristics of surface species in some Cr loading range.

3.6. The correlation between the structures of supported chromia catalysts and their catalytic performances for C_{10}+ aromatics hydrodealkylation

Table 8 gives the C_{10}+ conversion caused by unit Cr loading below monolayer coverage on SiO_2 and Al_2O_3. It can be found that CrO_x activity on the SiO_2 is higher than that on Al_2O_3.

Table 8
Conversion variation of CrO_x loading below monolayer on Al_2O_3 and SiO_2 carriers

Al_2O_3			SiO_2		
Cr contents (Cr/nm^2)	Conversion[a] (mol%)	Conversion[b] increasing (mol h^{-1} mol^{-1})	Cr contents (Cr/nm^2)	Conversion[a] (mol%)	Conversion[b] increasing (mol h^{-1} mol^{-1})
0.55	9	2.90	0.15	10.7	6.83
1.65	19.4	2.14	0.29	24.5	7.87
2.76	26.9	1.83	0.59	27.4	4.47
4.41	27.8	1.23			

[a] Had been subtracted the carrier conversion.
[b] Unit Cr loading.

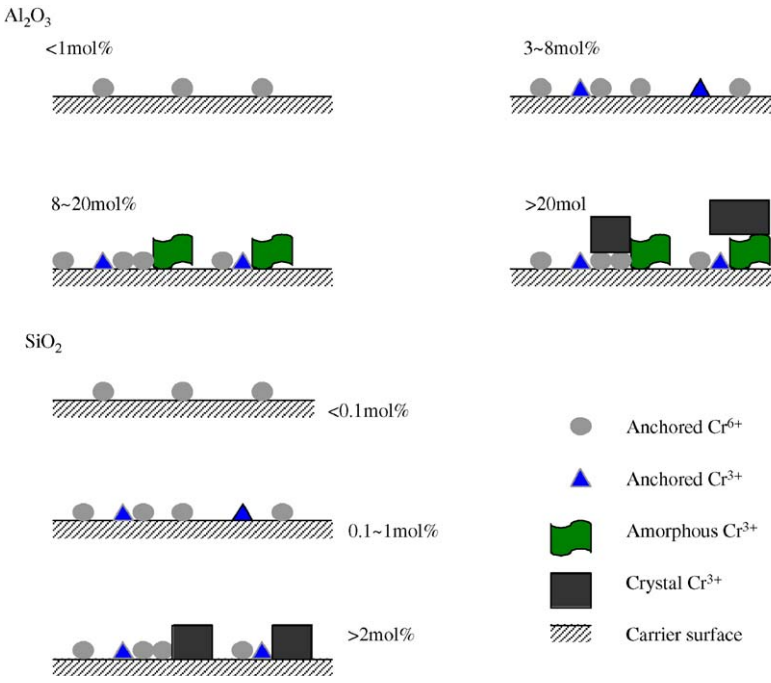

Fig. 7. Structural model of CrO_x species on Al_2O_3 and SiO_2 surfaces.

This may be due to the strong interaction between the active species and the support, which promotes the activation of aromatic effectively. It is believed that on lower Cr loading the C_{10}+ conversion normalized to molar Cr is higher than on higher Cr loading, except for the SiO_2 carrier. One of the reasons is because that isolated CrO_x species are difficult to be reduced, and the activity just comes from the reduced surface species. The other one is because that polychromium oxides are more active than the isolated ones. Also from the results in Tables 2 and 3, little difference was found in the C_6 aromatics concentrations in products, but large difference was observed in the C_9 aromatics concentrations. It indicates that alkyl with short chain or low subchain is difficult to be dealkylated and the CrO_x species are less effective to activate the light aromatics.

Based on the results in the present work, a structural model was proposed for the alumina- and silica-supported chromium oxide catalysts after calcination. This model is illustrated in Fig. 7. At low chromium loading the grafted Cr^{6+} is the predominant species, which anchors to the support probably through –OH groups randomly distributed on the support surface existing in mono-, di- or poly-chromates. The surface coverage increases with the spreading of a Cr^{3+} oxide, which are stabilized by interaction with the support through –OH groups. For alumina support, further addition of chromium oxide until the loading amount exceeds the monolayer coverage, amorphous Cr^{3+} oxide is formed, and finally, Cr_2O_3 builds up over the underlying dispersed chromium species as the Cr loading further increasing. But for silica support, the CrO_x species interact weakly with the support except for those anchored on the support more probably through –OH groups. They mainly exist in crystalline Cr_2O_3 state on support surface and do not form the amorphous Cr^{3+} oxides.

4. Conclusions

(1) Different supports (i.e. SiO_2, Al_2O_3) have large effects on the CrO_x oxide surface structures of supported chromia catalysts. CrO_x on the carrier surface may exist in different states, which relates to the carrier type. They may exist in anchored Cr^{6+}, anchored Cr^{3+}, amorphous or crystalline state. The anchored Cr is the best active site for C_{10}+ hydrodealkylation. The monolayer coverage of CrO_x are around 4.41 and 0.59 Cr/nm^2, on Al_2O_3, SiO_2, respectively.
(2) Surface CrO_x is the active species for hydrodealkylation, so the activity is the best for the catalysts with monolayer coverage of CrO_x.
(3) Different carrier-supported chromia catalysts have large effects on the catalytic performances for the hydrodealkylation of C_{10}+ aromatics. The conversions of C_{10}+ aromatics over SiO_2-supported chromia catalysts are higher than those over Al_2O_3-supported ones.

Acknowledgements

This work was supported by the National Natural Science Foundation of China (No. 20373043), the Scientific Research Key Foundation for the Returned Overseas Chinese Scholars of State Education Ministry, and the National Basic Research Program of China (Grant No. 2004CB217806).

References

[1] A.H. Wu, C.A. Drake, US Patent 6,509,289 B1 (2003).
[2] A.H. Wu, C.A. Drake, Drake, US Patent 5,856,609 (1999).
[3] A.H. Wu, C.A. Drake, US Patent 6,037,302 (2000).

[4] F.P. Daly, F.C. Wilbelm, US Patent 4,436,836 (1984).
[5] A.H. Wu, C.A. Drake, US Patent 5,763,721 (1998).
[6] G. Bjornson, US Patent 4,189,613 (1980).
[7] J.P. Brunelle, US Patent 4,247,730 (1981).
[8] T. Tsutsui, O. Kubota, US Patent 5,053,574 (1991).
[9] G. Bjornson, US Patent 4,331,566 (1982).
[10] F.P. Daly, F.C. Wilbelm, US Patent 4,451,687 (1984).
[11] G.J. Nacamuli, C.R. Wilson, R.F. Vogel, US Patent 6,051,744 (2000).
[12] A.H. Wu, C.A. Drake, US Patent 5,698,757 (1997).
[13] A.H. Wu, R.J. Melton, C.A. Drake, US Patent 5,929,295 (1999).
[14] A.H. Wu, C.A. Drake, R.J. Melton, US Patent 5,689,026 (1997).
[15] R. Alibeyli, A. Karaduman, H. Yeniova, A. Ates, A.Y. Bilgesu, Appl. Catal. A: Gen. 238 (2003) 279.
[16] D.C. Grenoble, J. Catal. 56 (1979) 32.
[17] D.C. Grenoble, J. Catal. 56 (1979) 40.
[18] S. Toppi, C. Thomas, C. Sayag, D. Brodzki, F.L. Peltier, C. Travers, G.D. Mariadassou, J. Catal. 210 (2002) 431.
[19] A.B. Gaspar, J.L.F. Brito, L.C. Dieguez, J. Mol. Catal. A: Chem. 203 (2003) 251.
[20] M.I. Zaki, N.E. Fouad, G.C. Bond, S.F. Tahir, Thermochim. Acta 285 (1996) 167.
[21] M.A. Vuurman, I.E. Wachs, D.J. Stufkens, A. Oskam, J. Mol. Catal. 80 (1993) 209.
[22] Z. Zhao, Y. Yamada, A. Ueda, H. Sakurai, T. Kobayashi, Catal. Today 93–95 (2004) 163.
[23] B.M. Weckhuysen, A.A. Verberckmoes, A.L. Buttiens, R.A. Schoonheydt, J. Phys. Chem. 98 (1994) 579.
[24] B.M. Weckhuysen, L.M.D. Ridder, R.A. Schoonheydt, J. Phys. Chem. 97 (1993) 4756.
[25] A.B. Lucas, J.L. Valverde, P. Canizayes, L. Rodriguez, Appl. Catal. A: Gen. 184 (1999) 143.
[26] M. Cherian, M.S. Rao, A.M. Hirt, I.E. Wachs, G. Deo, J. Catal. 211 (2002) 482.